JOURNAL OF OPTOELECTRONICS AND ADVANCED MATERIALS, Vol. 11, No. 8, August 2009, p. 1196 -1201

High temperature thermodynamic data of multiferroic ceramics based on $BiFeO_3$ – $BaTiO_3$ solid solutions

S. TANASESCU*, C. MARINESCU, A. SOFRONIA, A. IANCULESCU[a]
Institute of Physical Chemistry "Ilie Murgulescu" of the Romanian Academy, Splaiul Independentei 202, P.O. Box12-194, 060021 Bucharest, Romania
[a]*Polytechnics University of Bucharest, 1-7 Gh. Polizu, P.O. Box 12-134, 011061 Bucharest, Romania*

The coexistence of ferroelectricity and antiferromagnetism/weak ferromagnetism is responsible for the original magnetoelastic and magnetoferroelectric properties of $BiFeO_3$. In order to stabilize the single-phase composition and to improve the ferroelectric behaviour, the obtaining of binary solid solutions of $BiFeO_3$ with other perovskite type compounds with better dielectric and ferroelectric characteristics, as $BaTiO_3$ or $PbTiO_3$ seems to be a suitable approach. Taking into account the actual trend to eliminate the lead compounds from the industrial applications, our research was focused to the investigation of multiferroic lead-free ceramics based on the (1-x)$BiFeO_3$ - x$BaTiO_3$ ($0 \le x \le 0.30$) solid solutions. The samples were characterized by X-ray diffraction as single perovskite phases. The microstructures examined by scanning electron microscopy showed homogeneous ceramic surfaces. Differential scanning calorimetry experiments were performed in the temperature range of 500-900^{o}C in order to evidence the ferro-para phase transitions by a non-electrical method. Both the temperature and composition dependences of the specific heat capacity of the samples were determined and the variation of the Curie temperature with the composition was investigated. New features related to the thermodynamic stability of the multiferroic $BiFeO_3$ - $BaTiO_3$ ceramics were evidenced.

(Received January 26, 2009 after revision July 24, 2009; accepted August 05, 2009)

Keywords: Multiferroic ceramics, Perovskite, Thermodynamic properties, Defects

1. Introduction

A category of the most interesting multifunctional materials combining several properties in the same structure are the magnetoelectric multiferroics. Having simultaneous magnetic and ferroelectric activity, possible attractive functionalities caused by the interaction between the electric polarization and spontaneous magnetization were envisaged [1-3]. Among the single phase multiferroics, $BiFeO_3$ is one of the most studied systems in the latest years because of its spiral spin arrangement and ferroelectric ordering [4-8]. Already in the eighties, $BiFeO_3$ was proved as ferroelectric with the Curie temperature T_C around 830°C, antiferromagnetic with a high Néel temperature T_N (between 310 and 370°C), weak ferro/ferri magnetic in some temperature ranges, and also presenting a linear magnetoelectric effect [9-11]. Usually, small amounts of bismuth-rich secondary phase with controversial composition (corresponding either to $Bi_{40}Fe_2O_{63}$ or to $Bi_{36}Fe_2O_{57}$) and detrimental to the dielectric behaviour, were detected in the X-ray diffraction pattern of these ceramics. In order to enhance the stability of the perovskite phase with a beneficial influence on the dielectric and ferroelectric properties, the obtaining of some binary solid solutions with other perovskites compounds with good dielectric characteristics, as $BaTiO_3$ or $PbTiO_3$ seems to be a suitable approach [11-14].

Recent investigations using advanced techniques, motivated by the prospect of new applications, have uncovered rich complexities that had not previously been recognized, when the development of new multifunctional bismuth ferrite perovskites, that combine sensitive responses to electric, magnetic, and stress fields, is intended [15,16]. These phenomena occur at the crossover from localized to itinerant electronic behaviour and from FE to AFE displacive transitions, and are associated with dynamic, cooperative local deformations that are invisible to conventional diffraction studies. Due to the progress in methods for experimental analyzing distribution of elements at interfaces, some information has been accumulated on the chemical stabilities and properties of micro and nanostructured multifunctional materials. However the fundamental understanding was limited to rather simple cases. Such analyses need the thermodynamic data, because the driving forces for chemical reactions and diffusion can be given properly in terms of thermodynamic properties. This constitutes a considerable field of investigation, which is starting to be explored for both basic and applicative purposes [17-19].

In the present paper, new features related to the thermodynamic characterization of (1-x)$BiFeO_3$-x$BaTiO_3$ ceramics ($0 \le x \le 0.30$) prepared by solid state reaction following a two-step sintering procedure have been investigated. Particular attention is devoted to the high temperature thermodynamic data of these compounds for which the literature is rather scarce. The heat capacity data for the temperature range 700-900°C have been reported for the first time in this paper.

2. Experimental

2.1 Sample preparation

The compositions selected for this study are listed in Table 1.

Table 1. Composition of the specimens.

Sample	Composition
1	$BiFeO_3$
2	$Bi_{0.95}Ba_{0.05}Fe_{0.95}Ti_{0.05}O_3$
3	$Bi_{0.90}Ba_{0.10}Fe_{0.90}Ti_{0.10}O_3$
4	$Bi_{0.85}Ba_{0.15}Fe_{0.85}Ti_{0.15}O_3$
5	$Bi_{0.80}Ba_{0.20}Fe_{0.80}Ti_{0.20}O_3$
6	$Bi_{0.75}Ba_{0.25}Fe_{0.75}Ti_{0.25}O_3$
7	$Bi_{0.70}Ba_{0.30}Fe_{0.70}Ti_{0.30}O_3$

Samples with the mentioned composition were prepared by classical solid state reaction method from high purity oxides and carbonates: Bi_2O_3 (Fluka), Fe_2O_3 (Riedel de Haen), TiO_2 (Merck) and $BaCO_3$ (Fluka), as described earlier [20]. The presintering thermal treatment was carried out in air, at 650°C, with 2 hours plateau. The samples were slowly cooled, then grounded, pressed again into pellets and sintered in air for 1 hour at 800°C.

2.2 Sample characterization

X-ray diffraction measurements at room temperature, used to investigate the purity of the perovskite phase in the presintered powders, as well as in the sintered pellets were performed with a *SHIMADZU XRD 6000* diffractometer using Ni-filtered CuKα radiation (λ = 1.5418 Å), with a scan step of 0.02° and a counting time of 1 s/step, for 2θ ranged between 20° and 80°.

The microstructure of the ceramics was examined by scanning electron microscopy, using a Hitachi S2600N equipment.

The thermodynamic stability of the (1-x)$BiFeO_3$ – $x$$BaTiO_3$ ceramics in the temperature range from 500 to 900°C was investigated by using a *SETSYS Evolution Setaram* differential scanning calorimeter (DSC). Both the temperature and heat calibration of the calorimeter was carried out with National Institute of Standards and Technology (NIST) reference materials in the whole temperature range of the experiment. For the determination of heat capacity, NIST synthetic sapphire (SRM 742) was used as the reference material.

The DSC experiments were done on ceramic samples under the powder form, at a heating rate 10°C/min. and by using Ar with purity > 99.995% as carrier gas. The heat flow curves were processed with SETSOFT 2000 software. The critical temperatures corresponding to the ferro-para phase transitions and the corresponding enthalpies of transformations were obtained.

Experimental heat capacity was investigated for two temperature ranges: 550-675°C and 700-900°C. The method consists in performing three runs with two vessels: the measuring and the reference vessel. Two cylindrical alumina crucibles were used for the sample and reference cells. All three sets of experiments were performed under identical experimental conditions of heating rate and delay time, temperature range, and carrier gas flow rate. The first run is done with two empty vessels (blank test); in the second run the reference material (NIST synthetic sapphire) was loaded in the sample cell, and keeping the crucible in the reference side empty; in the third run a known weight of the sample was loaded in the sample cell, reference cell being empty. Each run consist in a ramp between the initial temperature T_i and the final temperature T_f at a constant heating rate (10°C/min). The expression used for the calculation of the heat capacity of the sample is given as:

$$Cp(T)_{sample} = \frac{HF_{sample} - HF_{blank}}{HF_{ref} - HF_{blank}} \frac{M_{ref}}{M_{sample}} Cp(T)_{ref} \qquad (1)$$

Here HF_{blank}, HF_{ref} and HF_{sample} represent the heat flow during the first, second and third runs respectively, $C_p(T)_{sample}$ and $C_p(T)_{ref}$ are the heat capacities of the sample and of the reference material [21] in J $K^{-1}g^{-1}$, and M_{sample} and M_{ref} represent the sample and reference mass, respectively. The heat capacity thus obtained was then converted to J $K^{-1}mol^{-1}$.

3. Results and discussion

The room temperature X-ray diffraction patterns obtained for the presintered samples show single-phase compositions (Fig. 1). The unique phase identified was the rhombohedral $BiFeO_3$ for the mixture 1, and the distorted rhomboedral $Bi_{1-x}Ba_xFe_{1-x}Ti_xO_3$ perovskite solid solutions for the mixtures no. 3, 5 and 7. The gradual change of the rhombohedral structure toward a cubic one with the increase of $BaTiO_3$ addition is proved by the disappearance of the X-ray diffraction splitting specific to pure $BiFeO_3$ [22].

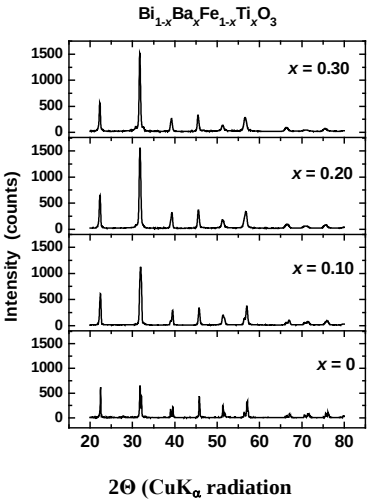

Fig.1. Room temperature X-ray diffraction patterns of $Bi_{1-x}Ba_xFe_{1-x}Ti_xO_3$ powders presintered at 650°C for 2 hours.

The processing procedure involving the first thermal treatment stage (presintering) performed on pressed samples and not on powdered mixtures and thus favouring complete chemical reactions may be responsible for the lack of Bi-rich non-equilibrium secondary phases.

Further investigations are required in order to calculate the lattice parameters and to determine the substitution degree at which the rhombohedral unit cell completely changes to a cubic symmetry.

SEM analyses were performed on the surface of the pellets calcined at 650°C/2 hours.

The SEM image of the $BiFeO_3$ sample (sample 1) shows that the ceramic consists of intergranular pores and of grains of various size (the average grain size was estimated to be ~ 20 μm), with not well defined grain boundaries, indicating an incipient sintering stage (Fig. 2).

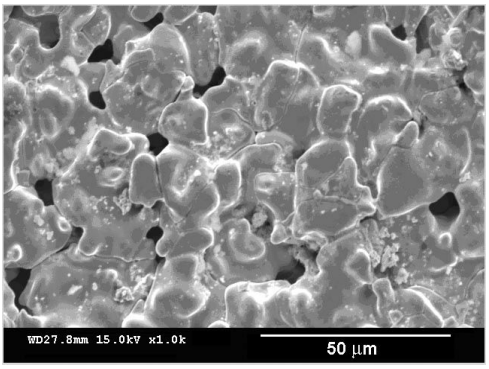

Fig. 2. Surface SEM image of $BiFeO_3$ sample thermally treated at 650°C for 2 hours.

The SEM images of samples 4 and 7 (Fig. 3, 4) show that the $BaTiO_3$ addition influences drastically the microstructure. One can observe the inhibiting effect of the barium titanate used as additive on the grain growth process and, consequently, a relative homogeneous microstructure, with a higher amount of intergranular porosity and grains with ~ one order of magnitude smaller than those ones of similar, non-modified sample, was formed, in both cases analyzed here.

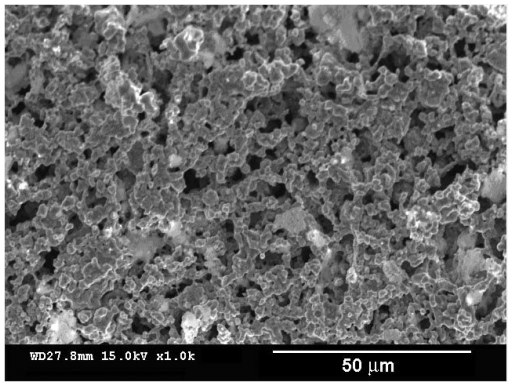

Fig. 3. Surface SEM image of $Bi_{0.85}Ba_{0.15}Fe_{0.85}Ti_{0.15}O_3$ sample thermally treated at 650°C for 2 hours.

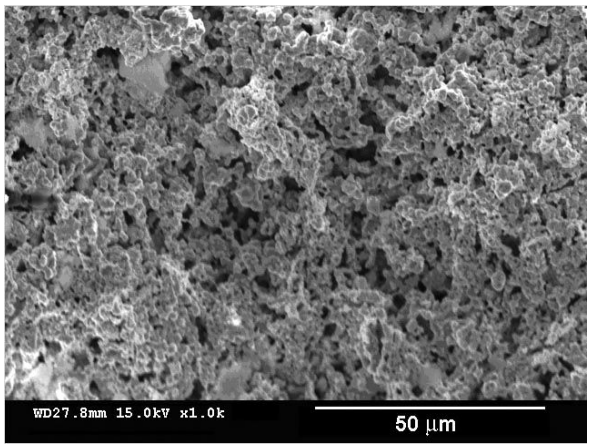

Fig. 4. Surface SEM image of $Bi_{0.70}Ba_{0.30}Fe_{0.70}Ti_{0.30}O_3$ sample thermally treated at 650°C for 2 hours.

Fig. 5 shows the raw DSC data as a function on the temperature and $BiFeO_3$ / $BaTiO_3$ ratio. The temperatures of phase transitions and the enthalpy change associated with the phase transition were obtained. The curve corresponding to $BiFeO_3$ indicates a phase transition at a temperature of 832°C. The T_c value obtained in this study is consistent with previous data indicating T_c values of about 820 - 850°C for $BiFeO_3$ [9, 10, 23].

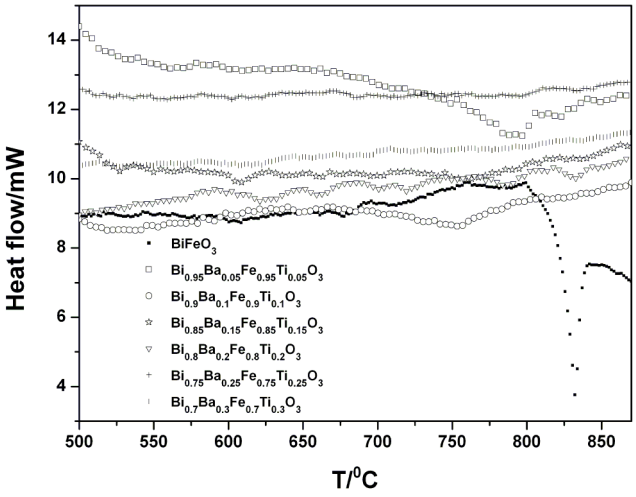

Fig. 5. DSC data as a function on the temperature and $BiFeO_3$ / $BaTiO_3$ ratio.

The effect of the $BaTiO_3$ addition to $BiFeO_3$ is seen as the decrease of the Curie transition temperature and of the corresponding enthalpy of transformation (Fig. 5). A sharp decline in the T_C was pointed out for $BiFeO_3$ rich compositions (Fig. 6). For the intermediate compositions ($x > 0.15$), the heat flow peaks are broadened, in consistence with the evolution of the XRD patterns. This behaviour could indicate the associated broad transition character in the substituted samples.

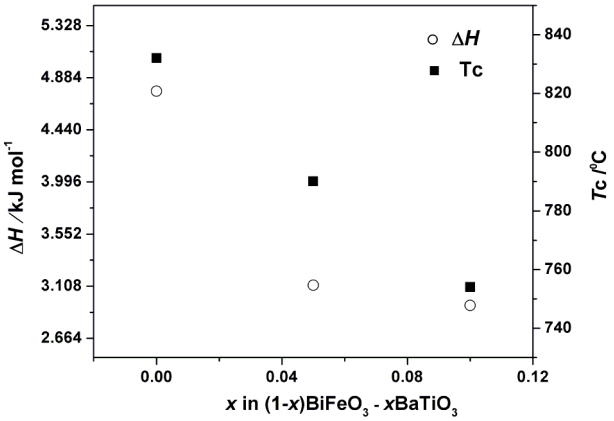

Fig. 6. Variation of the Curie transition temperature T_C and of the enthalpy of transformation for $BiFeO_3$ rich compositions (x=0; 0.05; 0.1).

However, the variation in the ferroelectric transition point is more evident from the heat capacity curves. In our study the *C*p values have been obtained in two different temperature ranges (i) 550-675°C and (ii) 700-900°C. For the first temperature range, the literature data are rather scarce. Only Phapale et al. [24] reported heat capacities of $BiFeO_3$ derived from the solution calorimetry and Calvet calorimetric data in the temperature range of 40-638°C. A comparison of our experimental results with the literature data can be made only for temperatures around 600°C. The results regarding the heat capacity values obtained in this work and for comparison those calculated from the temperature dependence of *C*p estimated by Phapale et al. [24] are listed in Table 2. One can observe that differences fall within the limits of the experimental errors and are mostly a consequence of the difference in the temperature range in which the estimated data from ref. 24 are valid.

Table 2. Comparison with previous data of the $BiFeO_3$ heat capacities at temperatures between 600 and 635 °C.

Temp. (^{0}C)	*C*p/Jmol^{-1}K^{-1}	
	This work	Calculated from ref. [24]
600	133.51	124.92
605	133.56	124.97
610	133.71	125.02
615	133.97	125.07
620	134.33	125.12
625	134.78	125.18
630	135.33	125.23
635	135.97	125.28

The heat capacity data for the temperature range 700-900°C have been reported for the first time in this paper. The ferroelectric (FE) to paraelectric (PE) transition is more obvious from *C*p curves. This is evident from Fig. 7 where comparative data of the *C*p and heat flow in the 700-900°C temperature range are presented.

A sharp decline in the T_C values of the $BiFeO_3$ rich compositions is also observed from the *C*p data. The *T*c decrease is accompanied by the reduction of the corresponding capacities values (Fig. 7, Table 3). In fact, the *C*p of the rhombohedral phase (x = 0) is obviously larger than that of the $Bi_{1-x}Ba_xFe_{1-x}Ti_xO_3$ perovskite phases, whereas the *C*p of each phase shows a weak composition dependence below the peak temperature.

In particular, the value of *C*p for x = 0.3 was found to be fairly low, which we did not show in the table.

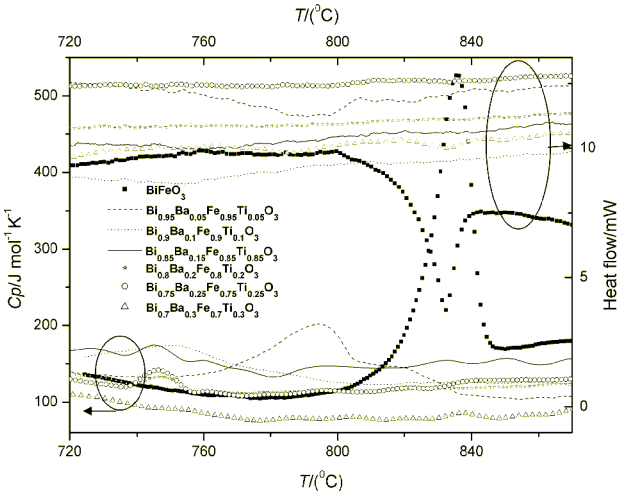

Fig. 7. Heat flow and Cp data (700– 900 ^{0}C temperature range).

Table 3. Heat capacities of the samples and the Curie transition temperature T_C.

Sample	T_C (^{o}C)	*C*p ($JK^{-1}mol^{-1}$)
$BiFeO_3$	836	526
$Bi_{0.95}Ba_{0.05}Fe_{0.95}Ti_{0.05}O_3$	794	202
$Bi_{0.90}Ba_{0.10}Fe_{0.90}Ti_{0.10}O_3$	752	175
$Bi_{0.85}Ba_{0.15}Fe_{0.85}Ti_{0.15}O_3$	745	175
$Bi_{0.80}Ba_{0.20}Fe_{0.80}Ti_{0.20}O_3$	746	142
$Bi_{0.75}Ba_{0.25}Fe_{0.75}Ti_{0.25}O_3$	746	133

The decreasing of the ferroelectric – paraelectric transition temperature with the increase of the $BaTiO_3$ amount in the composition of the solid solutions with x = 0 ÷ 0.15 indicated by the DSC measurements is in agreement with the dielectric data reported by Buscaglia et al [14].

Some reasons for this behaviour could be taken into account. First of all, these results confirm our observations that the solid solution system $BiFeO_3$ – $BaTiO_3$ undergoes structural transformations with increasing content of $BaTiO_3$. The decrease of the ferroelectric-paraelectric transition temperature T_c observed for the solid solution $(1-x)BiFeO_3 – xBaTiO_3$ may be ascribed to the decrease in unit cell volume caused by the $BaTiO_3$ addition [11].

Addition of Ba^{2+} having empty p orbitals, reduces polarization of core electrons and also the structural distorsion. The low value obtained for *C*p at x = 0.3 is in accordance with the previous result indicating that ferroelectricity disappears in samples above x ~ 0.3 [12].

The diffused phase transitions for compositions with x > 0.15 could be explained in terms of a large number of A and B sites occupied by two different, randomly distributed cationic specimens in the perovskite ABO_3 lattice. Previous reports on the substituted lanthanum manganites indicate that the mismatch at the A site creates strain on grain boundaries which affect the physical properties of an ABO_3 perovskite [25]. Besides, the role of charge ordering in explaining the magnetotransport properties of the variable valence transition metals perovskite was emphasized [19,26]. Investigating the influence of the dopants and of the nonstoichiometry on spin dynamics and thermodynamic properties of the magnetoresistive perovskites, Tanasescu et al [19, 27] pointed out that the remarkable behaviour of the substituted samples could be explained not only qualitatively by the structural changes upon doping, but also by the fact that the magneto-transport properties are extremely sensitive to the chemical defects in oxygen sites.

Though the effects of significant changes in the overall concentration of defects is not fully known in the present system of materials, extension of the results obtained on substituted manganites, may give some way for the correlation of the electrical, magnetic and thermodynamic properties with the defect structure. The partial replacement of Bi^{3+} with Ba^{2+} cations acting as acceptor centres could generate supplementary oxygen vacancies as compensating defects, whereas the Ti^{4+} solute on Fe^{3+} sites could induce cationic vacancies or polaronic defects by $Fe^{3+} \rightarrow Fe^{2+}$ transitions. The presence of the defects and the change of the Fe^{2+}/ Fe^{3+} ratio is in turn a function not only of the composition but equally importantly of the thermal history of the phase. The anionic vacancies created are masked by impurity conduction at low temperatures. As the temperature increases, impurity conduction ceases and conduction due to the oxygen vacancies will be evident. Consequently, an understanding of the high temperature defect chemistry of phases is vital, if an understanding of the low temperature electronic and magnetic properties is to be achieved.

To further evaluate these considerations, and in order to discriminate against the above contributions, the thermodynamic data could offer a valuable help. Further studies are in progress, so that experimental insight into the effects of defect types and concentrations on phase transitions to be examined.

4. Conclusions

$(1\text{-}x)BiFeO_3 - xBaTiO_3$ ($0 \le x \le 0.30$) ceramics were prepared by the solid state reaction method. After calcination at 650°C/2h and slow cooling, single phase compositions were obtained for all the mixtures analyzed. The gradual attenuation of the rhombohedral distortion with the increase of $BaTiO_3$ content was pointed out.

The $BaTiO_3$ admixture acts also as inhibitor for the grain growth process, contributing to the decrease of the average grain size.

Differential scanning calorimetry experiments were performed in order to evidence the ferroelectric-paraelectric phase transitions by a non-electrical method. Both the temperature and composition dependences of the specific heat capacity of the samples were determined and the variation of the Curie temperature with the composition was investigated. The temperatures of ferroelectric-paraelectric phase transitions and the corresponding enthalpies of transformations decrease with increasing concentration of $BaTiO_3$.

The reducing of the ferroelectric transition temperature with increasing concentration of $BaTiO_3$ confirmed the results of previous dielectric data.

New measurements are planned in order to evidence the influence of the oxygen stoichiometry change on the thermodynamic properties.

Acknowledgements

This work benefits from the support of the PNII-IDEAS program (Project nr. 50 / 2007).

Authors are also thankful to Prof. Liliana Mitoseriu from Department of Physics, Al. I. Cuza University Iasi, for helpful discussions and his critical reading of the manuscript.

References

[1] L. Mitoseriu, Bol. Soc. Esp. Ceram. **44**, 177 (2005).
[2] Y. Tokura, J. Magn. Magn. Mater. **310**, 1145 (2007).
[3] C. W. Nan, M. I. Bichurin, S. Dong, D. Viehland, G. Srinivasan, J. Appl. Phys. **103**, 031101 (2008).
[4] Y. P. Wang, L. Zhou, M. F. Zhang, X. Y. Chen, J. M. Liu, Z. G. Liu, Appl. Phys. Lett. **84**, 1731 (2004).
[5] K. Y. Yun, D. Ricinschi, M. Noda, M. Okuyama, S. Nasu, J. Kor. Phys. Soc. **46**, 281 (2005).
[6] J. Dho, X. Qi, H. Kim, J. L. MacManus-Driscoll, M. G. Blamire, Adv. Mater. **18**, 1445 (2006).
[7] G. L. Yuan, S. W. Or, Y. P. Wang, Z. G. Liu, J. M. Liu, Solid State Comm. **138**, 76 (2006).
[8] Y. H. Chu, Q. Zhan, L. W. Martin, M. P. Cruz, P. L. Yang, F. Zavaliche, S. Y. Yang, J. X. Zhang, L. Q. Chen, D. G. Schlom, I. N. Lin, T. B. Wu, R. Ramesh, Adv. Mater. **18**, 2307 (2006).
[9] I. H. Ismailzade, R. M. Ismailov, Phys. Status Solidi, A **59**, K191 (1980).
[10] P. Fischer, M. Polomska, I. Sosnowska, M. Szymanski, J. Phys. C. Solid State Phys. **13**, 1931 (1980).
[11] I. H. Ismailzade, R. M. Ismailov, A. I. Alekberov, F. M. Salaev, Phys. Stat Solidi. A **68**, K81 (1981).
[12] M. M. Kumar, A. Srinivas, S. V. Suryanarayana, J. Appl. Phys. **87,** 855 (2000).

[13] W. M. Zhu, Z. G. Ye, Ceram. Int. **30**, 1435 (2004).
[14] M. T. Buscaglia, L. Mitoseriu, V. Buscaglia, I. Pallecchi, M. Viviani, P. Nanni, A. S. Siri, J. Eur. Ceram. Soc. **26**, 3027 (2006).
[15] C. Ederer, N. A. Spaldin, Phys. Rev. B **71**, 224103 (2005).
[16] R. Ramesh, N.A. Spaldin, Nature Materials **6**, 1, 2007
[17] J. Maier, Solid State Ionics **291**, 154 (2002).
[18] S. Tanasescu, C. Marinescu, F. Maxim, Solid State Phenomena **99-100**, 117 (2004).
[19] S. Tanasescu, F. Maxim, F. Teodorescu, L. Giurgiu, J. Nanosci. Nanotechnol. **8**, 914 (2008)
[20] A. Ianculescu, L. Mitoseriu, H. Chiriac, M. M. Carnasciali, A. Braileanu, R. Trusca, J. Optoel. Adv. Mater. **10**, 1805 (2008).
[21] I. Barin, O. Knacke, Thermochemical properties of inorganic substances, Springer-Verlag, Berlin-Heidelberg-New York, 1973.
[22] F. Prihor, P. Postolache, L. Curecheriu, A. Ianculescu, L. Mitoseriu, Ferroelectrics, in press.
[23] F. Kubel, H. Schmid, Acta Crystallogr., Sect. B, Struct. Sci. **46**, 698 (1990)
[24] S. Phapale, R. Mishra, D. Das, J. Nuclear Materials **373**, 137 (2008).
[25] A. Maignan, C. Martin, H. Hervieu, B. Raveau, J. Hejtamanek, Solid State Commun. **107**, 363 (1998)
[26] G. H. Jonker, J. H van Santen, Physica **19**, 120 (1953).
[27] S. Tanasescu, M. N. Grecu, M. Urse, F. Teodorescu, L. M. Giurgiu, H. Chiriac, N. D. Totir, Advances in Applied Ceramics: Structural, Functional and Bioceramics, in press.

*Corresponding author: stanasescu2004@yahoo.com